A Large-Droplet Mode and Prognostic Number Concentration of Cloud Droplets in the Colorado State University Regional Atmospheric Modeling System (RAMS). Part II: Sensitivity to a Colorado Winter Snowfall Event

STEPHEN M. SALEEBY AND WILLIAM R. COTTON

Colorado State University, Fort Collins, Colorado

(Manuscript received 16 September 2004, in final form 18 June 2005)

ABSTRACT

This paper is the second in a two-part series describing recent additions to the microphysics module of the Regional Atmospheric Modeling System (RAMS) at Colorado State University. These changes include the addition of a large-cloud-droplet mode (40–80 μm in diameter) into the liquid-droplet spectrum and the parameterization of cloud-droplet nucleation through activation of cloud condensation nuclei (CCN) and giant CCN (GCCN). The large-droplet mode was introduced to represent more precisely the natural dual mode of the cloud-droplet distribution. The parameterized droplet nucleation replaces the former estimation of cloud-droplet formation solely from supersaturation calculations. In Part I of this series, details of the improvements to the microphysics were presented, including the set of equations governing the development of cloud droplets in the Lagrangian parcel model that was employed to parameterize this complex process. Supercell simulations were examined with respect to the model sensitivity to the presence and concentration of large cloud droplets, CCN, and GCCN. Part II examines the sensitivity of the model microphysics to imposed aerosol variations in a wintertime snowfall event that occurred over Colorado on 28–29 February 2004. Model analyses and sensitivity are compared with the real-time forecast version 4.3 of RAMS as well as selected snowpack telemetry (SNOTEL) accumulated precipitation data and surface data from Storm Peak Laboratory in Steamboat Springs, Colorado.

1. Introduction

In recent years the predictive capability of cloud bulk-microphysical models has been extended to include prognosis on two moments of the hydrometeor distributions: mixing ratio and number concentration (e.g., Ziegler 1985; Ferrier et al. 1995; Meyers et al. 1997; Reisner et al. 1998). The previous approach typically involved prediction of mixing ratio alone, which imposes constraints on the evolution of the hydrometeor spectrum (e.g., Hsie and Anthes 1984; Dudhia 1989; Tao et al. 1989; Walko et al. 1995; Hong et al. 1998; Souto et al. 2003). Early representations of hydrometer distributions, following that of Kessler (1969), required user specification of the slope or intercept parameter N_0 of a Marshall and Palmer (1948)-type exponential distribution. A more recent depiction of both liquid and ice spectra involves prescribing hydrometeor basis functions as gamma-type distributions that can evolve over time in a bin-microphysical sense (Clark and Hall 1983; Verlinde et al. 1990). Walko et al. (1995) introduced the microphysics model of the Colorado State University (CSU) Regional Atmospheric Modeling System (RAMS) in the framework of one-moment prediction, and Meyers et al. (1997) extended it to two moments of the distribution for rain, pristine ice, snow, aggregates, graupel, and hail. Autoconversion of cloud droplets to rain is treated according to a quasi-bin approach (Feingold et al. 1988), and heat diffusion and vapor diffusion of hydrometeors are specified according to Walko et al. (2000). The Meyers et al. (1997) version improved upon hydrometeor prognostic quantities, but it still prognosed only mixing ratio of the cloud-droplet distribution; as such, cloud-droplet nucleation was treated very simplistically. If supersaturated conditions exist, the excess vapor is condensed from the vapor phase to the liquid-droplet phase. The number concentration of newly formed droplets is diagnosed from the condensed water and a specified minimum

Corresponding author address: Stephen M. Saleeby, Atmospheric Science Department, Colorado State University, Fort Collins, CO 80523.
E-mail: smsaleeb@atmos.colostate.edu

droplet diameter of 2 μm. This formulation is currently used in the real-time version 4.3 of the RAMS model at CSU to produce daily forecasts.

Saleeby and Cotton (2004, hereinafter Part I) extended the two-moment approach to the cloud-droplet distribution through a parameterization for the formation of cloud droplets from activation of cloud condensation nuclei (CCN) and giant CCN (GCCN) within a lifted parcel. The Lagrangian parcel model of Heymsfield and Sabin (1989), based upon the Köhler equations for aerosol activation and the supersaturation equation for a lifted parcel (Pruppacher and Klett 1997), was utilized to determine the percent of user-specified CCN that would deliquesce, activate, and grow by condensation into cloud droplets. The equation set for parcel model integration of droplet growth is given in Part I.

The lookup table approach of Walko et al. (1995) was implemented to circumvent the need to couple the parcel model to the mesoscale model microphysics. The lookup tables are multidimensional data arrays whose values contain the percent of CCN that will result in the formation of cloud droplets within an environment that varies with temperature, vertical velocity, concentration of CCN, and median radius of the CCN distribution (Part I). The cloud-droplet spectrum was further modified to behave as a bimodal distribution with small cloud droplets (hereinafter referred to as cloud1) from 2 to 40 μm in diameter and large cloud droplets (hereinafter referred to as cloud2) from 40 to 80 μm in diameter. This bimodal representation of the cloud-droplet spectrum follows from observations of Hobbs et al. (1980) and Warner (1969) of a frequently occurring second peak in the droplet spectrum with diameters at the larger end approaching the size of drizzle droplets. The cloud2 mode is systematically implemented in the bin-model approach used in droplet sedimentation and in solutions to the stochastic collection equation for autoconversion of cloud droplets to rain (Tzivion et al. 1987; Feingold et al. 1988). This implementation requires growth to this intermediate-size droplet category before reaching rain sizes, thereby slowing the collection process to more realistic time scales. The parameterized activation of CCN (GCCN) and growth of their solution droplets results in direct formation of cloud1 (cloud2) droplets.

In terms of aerosol impacts, it is widely known that higher CCN concentrations tend to decrease cloud-droplet size, increase number concentration, and narrow the droplet spectrum (Warner and Twomey 1967; Fitzgerald and Spyers-Duran 1973; Pruppacher and Klett 1997). However, Johnson (1982) and Feingold et al. (1999) showed that, in warm clouds, GCCN can act to accelerate and increase rain formation by reducing the colloidal stability of the cloud through broadening of the droplet distribution and enhanced collisional growth. From observations, Mather (1991) concluded that advertent or inadvertent seeding of clouds by large hygroscopic nuclei may enhance the precipitation process by accelerated "coalescence or coalescence-freezing mechanisms," and that ice formation may aid in this enhancement. Aerosol influences are not limited to warm-cloud processes; it has been found that variability in aerosol concentrations can alter ice particle riming efficiencies (Hindman et al. 1994; Borys et al. 2000, 2003). To be more specific, Borys et al. (2000, 2003) found that increased sulfate-based aerosol concentrations suppress formation of larger cloud droplets and reduce riming of cloud droplets by ice hydrometeors. Pruppacher and Klett (1997) delineate 10 μm to be the cloud-droplet riming cutoff radius below which riming efficiencies are near zero. It is largely this alteration of cloud-droplet properties and ice particle riming that we will examine within this modeling study.

This study involves the simulation of a local, winter snowfall event over Colorado that occurred from 28 to 29 February 2004. This case represents a classic, northwesterly-flow, high-mountains snowfall event for northern Colorado. It provides an excellent test case for examining the sensitivity of the new cloud-droplet parameterization to the initial aerosol concentration and to cold-cloud processes. It also serves as a comparison with the daily-run real-time RAMS model to assess any improvement to forecasts of precipitation and snow water equivalent brought about by updating the cloud-droplet parameterization.

During this case of 28–29 February 2004, northern Colorado was generally under a northwesterly flow regime as a low pressure system moved in from Utah. The main low pressure center split once it reached western Colorado; the southern low crossed the Four Corners region, and the northern low passed over southern Wyoming. The low in southern Wyoming was the main weather maker for northern and central Colorado. Substantial snow amounts (>45 cm) occurred over the higher terrain of the foothills and major mountain ranges west of the Front Range while relatively little precipitation fell over the eastern plains of Colorado. This case was chosen because the authors were present, during the snow event, at the Desert Research Institute's Storm Peak Laboratory (SPL), which is located at the summit of Mount Werner in Steamboat Springs, Colorado. The forecast version of RAMS was also run in real time for this event; the current real-time model version is identical to the version being tested here,

with the exclusion of the new cloud-droplet parameterization.

In this investigation, a series of sensitivity test simulations with varying number of prognostic moments and initial CCN and GCCN concentrations was performed (see Table 1; expt 1 was run with the standard real-time RAMS model cloud-droplet parameterization). The focus of this paper is 1) to examine the model variability in total and individual hydrometeor-type precipitation accumulations; 2) to examine the variability in microphysical processes as they relate to droplet and ice nucleation, vapor growth, growth and transfer by collection, melting of ice, and evaporation of ice and liquid hydrometeor types; and 3) to assess whether the new cloud-droplet parameterization provides improved forecasting skill. This assessment includes a budget study of the relative variation in the sources and sinks of each hydrometeor class.

Although observational comparisons are not our primary focus, we briefly compare model output with 5-min data of general meteorological fields measured atop a tower located on the roof of SPL to make a broad assessment of the forecast ability in this case. Furthermore, modeled snow water equivalent accumulation is compared with observations from several snowpack telemetry (SNOTEL) sites over north-central Colorado.

2. Model setup

All simulations performed in this study were configured according to the specifications of the current RAMS prototype real-time forecast model. This nonhydrostatic, compressible version of the model is configured on an Arakawa-C grid and sigma-z terrain-following coordinate system (Pielke et al. 1992; Cotton et al. 2003). The model uses two-way nesting with a three-grid arrangement for this particular application (see Fig. 1). The outer grid 1 covers the continental United States with a 48-km grid spacing (100 × 72 grid points, 60-s time step), the nested grid 2 covers Colorado and portions of the adjacent surrounding states with a 12-km grid spacing (78 × 72 grid points, 20-s time step), and a nested grid 3 encompasses much of Colorado with a 3-km grid spacing (98 × 98 grid points, 6.67-s time step). Within each grid there are 32 vertical levels with a minimum of 300-m grid spacing near the surface; the model uses vertical grid stretching with a stretch ratio of 1.1 and a maximum vertical grid spacing of 750 m in the upper and midtroposphere.

For these simulations, the model was initialized at 0000 UTC 28 February 2004 and was run for 39 h, which spans the time period of observations obtained at SPL in real time. The four-dimensional data assimilation initialization files were an assimilation of the Eta Model 40-km 6-hourly forecast grids over the continental United States. Lateral boundary nudging files were created at 3-h intervals on 17 pressure levels, and boundary forcing was imposed at a 15-min time scale on the five outermost lateral grid points, with exponentially decreased forcing toward the inner grid points. The Kain–Fritsch cumulus parameterization was employed on the two outermost grids where the grid spacing is insufficient to resolve small-scale convection explicitly (Kain and Fritsch 1990, 1992, 1993). Turbulent diffusion was imposed according to Smagorinsky (1963) for the horizontal plane and by the level-2.5 prognostic turbulent kinetic energy closure scheme of Mellor and Yamada (1974) in the vertical direction.

The base-state simulations were run with two-moment microphysics prognosing hydrometeor mixing ratio and number concentration for rain, pristine ice, snow, aggregates, graupel, and hail. Two-moment prediction was implemented selectively for the two cloud-droplet modes. Initial CCN and GCCN concentrations were user specified and vary between simulations, as given in Table 1. In each simulation a number concentration for CCN and GCCN was specified at the start time, and the 3D field was initialized homogeneously. Source and sink terms for the aerosols are active following initialization. The aerosol concentrations are represented by a polydisperse field on a lognormal distribution (see Part I) with a median radius for CCN (GCCN) of 0.04 μm (3.0 μm). Ice nuclei (IN) were activated according to the formulation of Meyers et al. (1992), with a maximum background concentration of

TABLE 1. Variations in experiment initial conditions. All simulations were identical except for the variations shown here. The simulations used a CCN (GCCN) median radius of 0.04 μm (3.0 μm). CCN nucleate into the small-droplet mode (cloud1, 2–40-μm mean diameter), and GCCN nucleate into the large-droplet mode (cloud2, 40–80-μm mean diameter). Aerosol concentrations were initialized as 3D homogeneous.

	No. of predicted moments		No. concentration (cm^{-3})	
Expt	Cloud1	Cloud2	CCN	GCCN
1	1	0	—	—
2	1	1	—	—
3	2	1	100	—
4	2	2	100	0.010 00
5	2	2	100	0.000 01
6	2	1	500	—
7	2	2	500	0.010 00
8	2	2	500	0.000 01
9	2	1	1000	—
10	2	2	1000	0.010 00
11	2	2	1000	0.000 01

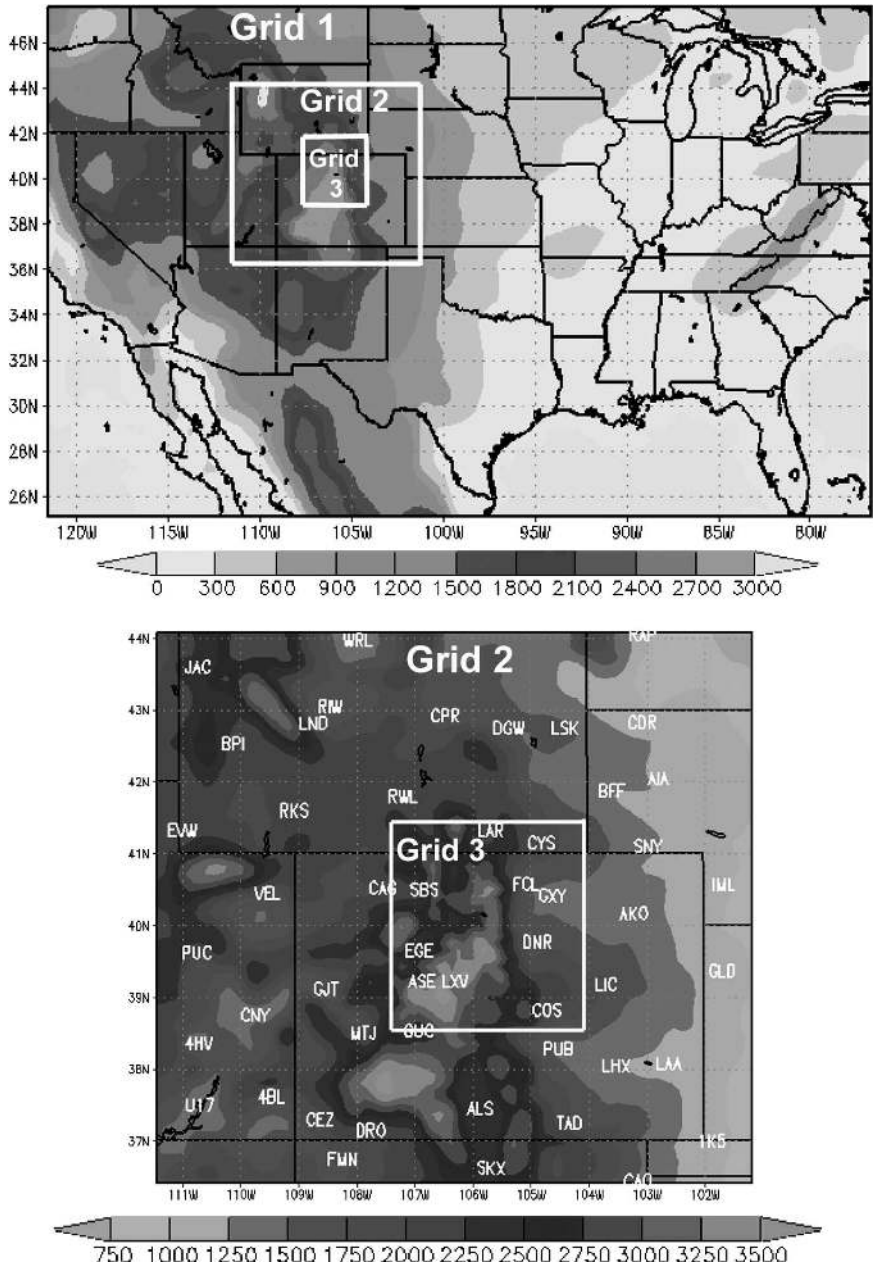

FIG. 1. Real-time RAMS grid configuration displaying (top) the outer and nested grids, and (bottom) a zoomed display of the two inner grids and their boundaries relative to local cities in CO and surrounding states. Topography (m) is overlaid.

10^5 kg^{-1} that decreases aloft as a function of air density. Ice crystal nucleation from IN, according to the Meyers et al. formula, is a function of supersaturation with respect to ice.

3. SPL observations and model comparison

The meteorological data from SPL were recorded as 5-min averages and include temperature, dewpoint, relative humidity, wind speed, wind direction, precipitation, and air pressure, among the total measured fields. The model analysis files for each experiment were output less frequently than the SPL data and are available in 15-min intervals. For a time series comparison with the SPL observations, the closest model grid to SPL was extracted from the model output at each analysis time and was interpolated to the height of SPL. The resulting overlaid time series plots are shown in

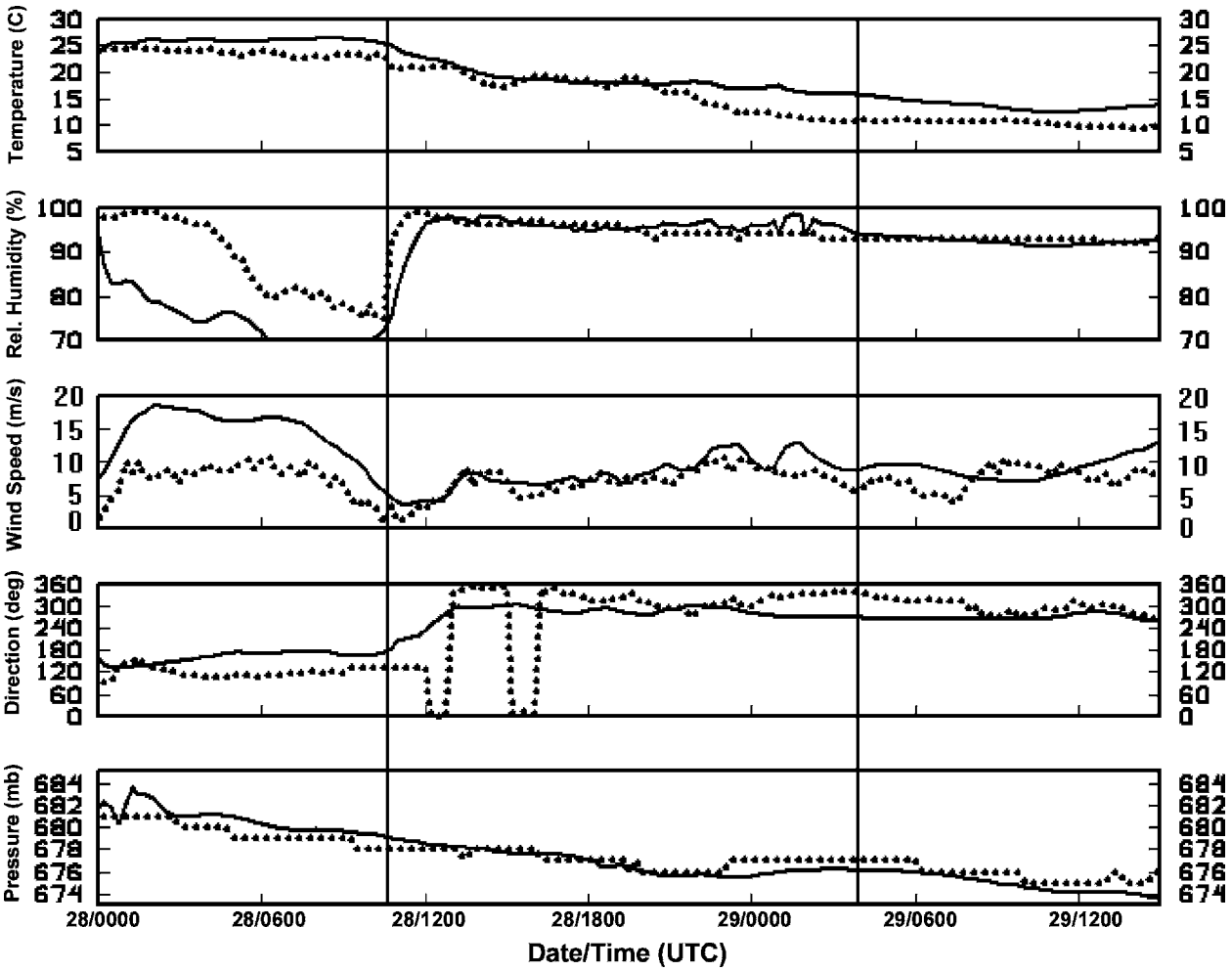

FIG. 2. Time series of meteorological observations from SPL (dotted line) and a representative corresponding RAMS time series of the closest gridpoint values interpolated to the elevation of SPL (solid line).

Fig. 2 for SPL and a single representative simulation. Despite the estimations inherent in vertical interpolation of the closest gridpoint data over such complex terrain, the simulations generally perform well in forecasting the temporal variability and magnitude of surface temperature and pressure at the SPL location. The plots of relative humidity and wind speed and direction deviate from the observations within the first 12 h but then agree more closely with observed conditions for the duration of the event. The early deviation is not unexpected because the model requires spinup time to establish equilibrium among the thermodynamic, dynamic, and microphysical variables following the Eta initialization over this complex terrain.

The largest intersimulation variability that is present after spinup exists in the time series of relative humidity and wind speed for the time period from 1000 UTC 28 February to 0300 UTC 29 February. Overlaid plots of these time series for all simulations and SPL are displayed in Fig. 3. In the plot of relative humidity, all of the simulations reveal a 1–2-h time lag in the abrupt increase in RH that preceded the onset of snowfall at SPL. As noted on this plot, experiments 4 and 8 exhibit the maximum variability, with temporary deviations from the observed RH of up to 15%–18%; in general, the observed RH varied very little. It is difficult to isolate the reasons for the variability in RH at this one location, because of complex interactions among the dynamics, thermodynamics, and topography, but part of the variability can be attributed to differences in cloud formation and mixing ratio over the SPL site resulting from varying the initial aerosol concentration. Fluctuations in droplet nucleation, vapor growth, and evaporation resulting from changes in the aerosol concentration produce variations in the local RH at the surface at SPL. Less variability was present in the wind

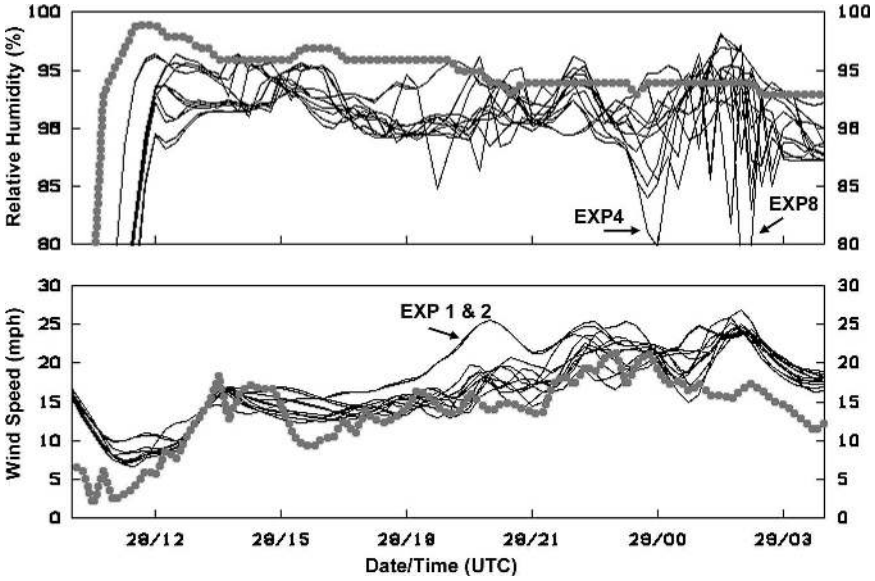

FIG. 3. Zoomed-in time series of (top) relative humidity (%) and (bottom) wind speed ($m\ s^{-1}$) for the subsection of Fig. 2 between the two vertical lines. SPL observations (thick gray line) and the composite of the RAMS simulations (thin black lines) display the range of model realizations. Several particular perturbations are noted on the plots.

speed time series among simulations and between the simulations and observations. The variability in wind speed may be partly related to variations in droplet nucleation in terms of the release of latent heat during condensation. Variations in parcel buoyancy resulting from condensation and evaporation could affect horizontal and vertical motion. The main outliers among the simulations were experiments 1 and 2, both of which use the standard real-time model formulation for cloud-droplet formation. The simulations initialized with CCN and/or GCCN agree more closely to the SPL wind speeds.

4. Precipitation accumulation

a. Model precipitation

The modeled time series of accumulated precipitation from all of the simulations as well as from the Steamboat Springs Ski Patrol Station Headquarters (STM) and the Rabbit Ears Pass SNOTEL station are shown in Fig. 4. Each of the time series in this figure begin accumulation near 1000 UTC 28 February and run through the final time at 1500 UTC 29 February. Despite the different model initializations of aerosols and cloud droplets, all of the simulations perform well

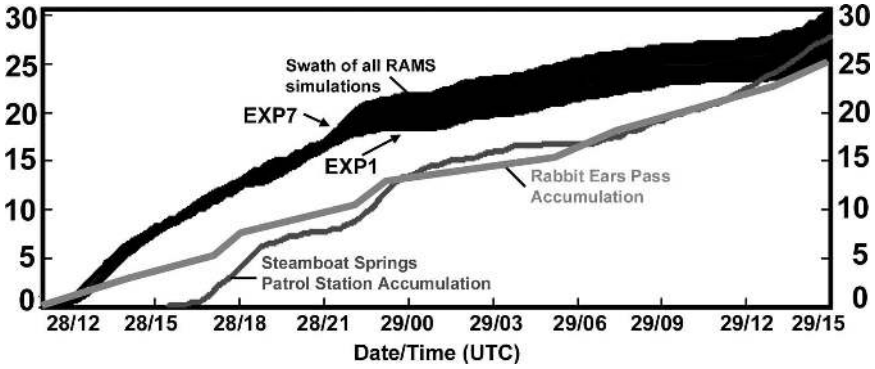

FIG. 4. Time-accumulated liquid equivalent precipitation (mm) from RAMS simulations (dark filled region; this encompasses the range of precipitation time series from all experiments), the Steamboat Springs ski resort precipitation gauge (dark gray line), and the nearby Rabbit Ears Pass SNOTEL site (light gray line).

in forecasting the accumulation of the liquid equivalent snowfall by the end of the time period. The main difference between the simulations and observations is in the onset of precipitation. The simulations tend to initiate precipitation 3–4 h earlier than that observed at STM. The earlier-than-observed onset of precipitation in the model may be partially due to an early transition from southerly to westerly flow in the model relative to that observed (see Fig. 2d). The wind shift initiated prematurely forecast upslope flow along the north–south-oriented Park Range, in which SPL is situated. In the presence of ample moisture, such a wind transition is highly favorable for precipitation formation along this mountain range. Also of consequence is a time lag in the reporting of precipitation from the STM tipping-bucket gauge. The tipping-bucket gauge is known to produce accurate precipitation measurements, but occasionally there exists an unfortunate time lag in the reporting of precipitation at the time of onset (R. Borys 2004, personal communication). If the time lag is indeed on the order of several hours, it may certainly account for the discrepancy between the model and observations. In either case, the final accumulation magnitudes closely agree by 1500 UTC 28 February. Among the simulations, there exists a variability of 5 mm (~20%) in total accumulated precipitation at Steamboat Springs. The variability in precipitation across the ensemble of simulations reveals the potential influence of pollution effects and suggests the need for future improved initialization of aerosols from observations so as to improve model forecasting skill.

Liquid equivalent precipitation data from several SNOTEL sites in Colorado were also used for model comparison and for examination of model variability. These stations automatically record precipitation data periodically, although the frequency of measurements is anywhere from 1 to 24 h. Eight sites that are familiar to the authors, with frequent reporting times, were chosen for comparison, and their locations are displayed on each panel in Fig. 5. These stations are Bison Lake (BIS), Rabbit Ears Pass (RAB), Vail Pass (VAL), Joe Wright Reservoir (JOE), Bear Lake (BEA), Lake Eldora (ELD), Independence Pass (IND), and Loveland Basin (LOV). These sites are located along different mountain ranges and were chosen to assess the model variability among simulations and the model's ability to forecast precipitation along varying topography. Table 2 displays the simulation-accumulated precipitation at the closest model grid point to each site for each sensitivity test as well as the observed values. The SNOTEL sites received only frozen precipitation, though they report the liquid equivalent amount. The variance and standard deviations are given for the forecast at each station to assess the range of model forecasts, and the root-mean-square difference (RMSD) is given to examine the performance of each simulation against the observations from all SNOTEL sites.

The first point to note is that, from Table 2, there is no single simulation that provides the best forecast in precipitation accumulation for every SNOTEL site. For example, experiments 1 and 2 are closest to the observed values at BIS, whereas they comparatively produce the worst forecast at VAL. The RMSD values were calculated for each experiment against the observations at the nine reporting sites. The RMSD was also computed for the average of the accumulations from the experiments that utilize the aerosol parameterization. These values indicate that experiment 5 (expt 10) performed the best (worst) with regard to forecasting snow water equivalent at these SNOTEL sites. The RMSD of the average of the aerosol ensemble runs (expts 3–11) outperformed the experiments using the default cloud-droplet parameterization (expts 1–2). The relative variability in precipitation among simulations at each location also provides insight into the magnitude of the impact of aerosols/pollution. The range of precipitation extremes at the SNOTEL sites reveals a variation up to 30% depending upon the model initialization of aerosol and cloud droplets.

To put into perspective the variability in the total precipitation produced over the course of these 39-h simulations, we briefly compare the modeled precipitation with the treated water usage for the city of Denver and for Colorado as a whole. This exercise provides a real-world application of the potential impacts of pollution (through CCN/GCCN) upon the total surface water that accumulates from a single storm system and how that can influence the general public. On average, Colorado residents consume 865×10^6 m^3 of treated water per year, and in Denver alone 288×10^6 m^3 of water is consumed (information was obtained online at www.denverwater.org). Among the simulations, this single modeled snowstorm produced precipitation amounts totaling 903, 933, and 989×10^6 m^3 of surface precipitation accumulated over the whole of grid 3 from experiment 1 (default droplet scheme, essentially very polluted), experiment 11 (polluted), and experiment 5 (nonpolluted), respectively. This single storm alone could provide more than one year's water supply if it could all be stored; furthermore, the maximum range of surface water for this one case amounts to nearly 86×10^6 m^3. This variability of ~10% amounts to nearly one-third of Denver's yearly water consumption. Even a 10% reduction in precipitation over a large area because of enhanced pollution could influence the regional water supply.

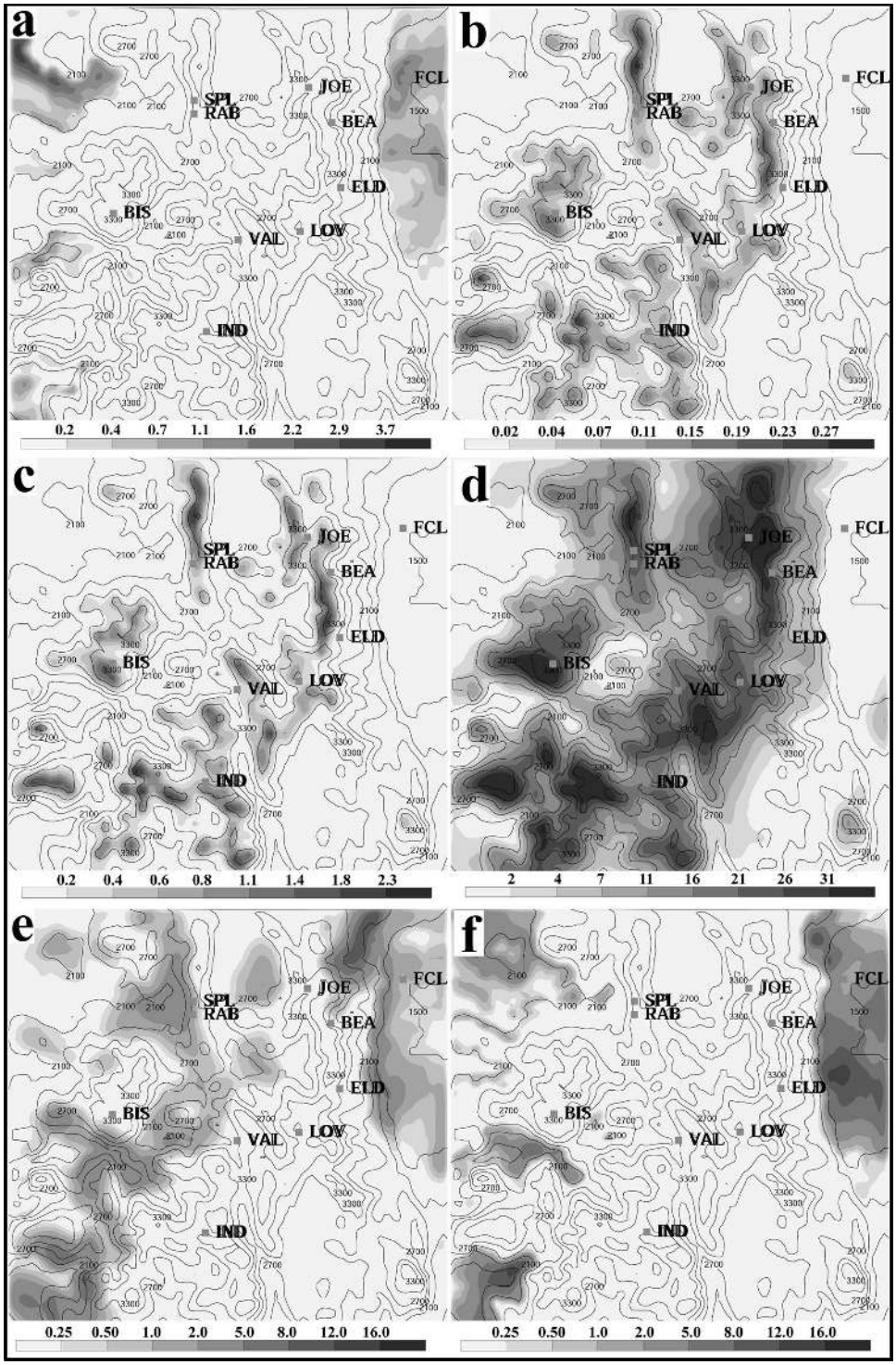

FIG. 5. Total liquid equivalent accumulation (mm) of (a) rain, (b) pristine ice, (c) snow, (d) aggregates, (e) graupel, and (f) hail from 0000 UTC 28 Feb to 1500 UTC 29 Feb from experiment 8, with CCN and GCCN concentrations of 500 and 10^{-2} cm^{-3}, respectively. Topography (m) and SNOTEL locations are overlaid.

TABLE 2. Accumulated liquid equivalent precipitation (mm) from STM and SNOTEL sites for each simulation. The SNOTEL sites are defined in section 4a. RMSD for each experiment over all stations is given in the rightmost column. The row labeled 3–11 avg gives the average values of the ensemble of simulations that made use of the aerosol parameterization.

Expt	STM	BIS	RAB	VAL	JOE	BEA	ELD	IND	LOV	RMSD
1	25.91	29.46	25.40	24.89	36.32	22.86	15.24	17.99	22.65	4.83
2	25.91	29.46	25.40	25.15	36.07	22.86	14.99	17.78	22.18	4.75
3	27.94	36.07	23.62	19.81	30.23	18.80	13.21	20.57	22.31	4.73
4	27.18	35.56	22.86	20.57	31.75	19.30	11.43	19.31	21.17	4.47
5	28.19	35.56	24.13	18.03	31.50	20.32	13.46	20.32	20.36	4.63
6	30.73	36.32	26.92	21.84	35.31	19.81	10.16	21.35	19.30	4.77
7	29.72	35.56	25.91	21.84	32.51	22.35	12.19	17.21	24.61	5.14
8	29.46	37.08	26.42	19.30	32.77	20.07	13.46	20.03	17.32	4.56
9	27.18	35.31	24.89	20.57	31.24	22.86	13.97	18.02	25.15	5.42
10	28.70	35.81	25.40	18.29	32.26	23.62	15.49	19.31	22.63	5.48
11	26.67	35.56	24.38	19.56	34.80	21.84	13.46	20.05	23.11	5.15
3–11 avg	28.42	35.87	24.95	19.98	32.48	21.00	12.98	19.57	21.77	4.69
Obs	28.19	27.94	27.94	20.32	33.02	12.70	12.70	15.24	17.78	
Closest to obs	Expt 5	Expts 1 and 2	Expt 6	Expts 4 and 9	Expt 7	Expt 4	Expts 3 and 7	Expt 7	Expt 8	
Max − min	4.83	7.62	4.06	7.11	6.10	4.83	5.33	4.14	7.83	
Variance	2.50	6.96	1.46	5.65	4.42	2.90	2.65	1.80	5.14	
Std dev	1.58	2.64	1.21	2.38	2.10	1.70	1.63	1.34	2.27	

b. Surface precipitation spatial distributions

Plotted fields of the accumulation of the dominant hydrometeor type provide insight into the relative contributions of each species to the total precipitation. Figure 5 displays the maximum accumulation of rain, pristine ice, snow, aggregates, graupel, and hail from experiment 8, with CCN and GCCN concentrations of 500 and 10^{-2} cm^{-3}, respectively. (In these simulations, hail is formed from frozen rain or partially melted graupel.) This simulation was chosen as an example to display the spatial fields of hydrometeor accumulation. Among simulations, the spatial patterns of accumulated hydrometeor type are similar while the variability in magnitude varies more substantially depending upon the initial aerosol concentration.

There are several key points to note from Fig. 5. Rainfall is specifically limited to the lower elevation of the northern Front Range of Colorado, as well as the lower valleys and plains along the western edge of the state. No rain accumulation occurs above 1800 m MSL. Accumulations of pristine ice and snow are solely limited to the highest elevations (above 2400 m) along the individual mountain ranges. Aggregates account for the majority of all accumulation above the freezing level (above 1800 m). The swath of aggregate accumulation covers all of the mountain ranges, the eastern and western slopes, and the foothills of Colorado. The spatial pattern of graupel is less specific than the other hydrometeor species. Accumulations occur along the Front Range urban corridor and over nearly all of the northern and western mountains and foothills. There is a large gap in graupel over the south-central and southeast portions of the domain; the gap region is the largest continuous region of high terrain above 2400 m. Above this elevation not enough liquid water was present for substantial riming growth of graupel. The spatial pattern of hail is very similar to that for rain and is located solely at the lower elevations. This pattern occurs because hail primarily grows by collection of rain or melting graupel, and it may melt below the freezing level to become rain.

In the following sections, many of the tables and charts that are discussed provide information concerning domain-summed or domain-averaged quantities. It is useful to keep in mind the general spatial fields of accumulated hydrometeor types when interpreting the results that are shown. For example, a domain-averaged quantity of accumulated rain will receive its primary contribution from accumulation along the Front Range (see Fig. 5).

c. Cloud-droplet characteristics

Cloud1 droplet mixing ratio, number concentration, and mean diameter vary among simulations because of the variability in initial CCN and GCCN concentrations. Aerosol concentrations directly determine the nucleation rate of cloud droplets in the model, and the variability in cloud-droplet properties influences growth of the remaining hydrometeor types. Table 3 displays the averaged cloud-droplet characteristics among sensitivity experiments. The averaging of droplet properties was done for only those grid points with cloud water mixing ratio greater than a minimum threshold of 0.0001 g kg^{-1}. In general, as the concentration of CCN is increased, the cloud1 mixing ratio and

TABLE 3. Domain-averaged and time-averaged quantities for the cloud1 droplet mode. Only grid points with cloud1 mixing ratio greater than 0.0001 g kg^{-1} were considered.

Expt	Cloud1 mixing ratio (g kg^{-1})	Cloud1 concentration (No. cm^{-3})	Cloud1 mean diameter (μm)
1	0.0439	—	—
2	0.0435	—	—
3	0.0094	0.68	36.28
4	0.0073	0.77	34.30
5	0.0092	0.67	36.24
6	0.0117	4.35	29.79
7	0.0111	4.70	28.80
8	0.0117	4.35	29.80
9	0.0113	11.13	24.88
10	0.0098	11.75	24.16
11	0.0109	10.96	25.06

number concentration increase while the mean diameter decreases. When GCCN concentration is increased, the cloud1 mixing ratio and mean diameter decrease slightly and the number concentration increases. The one exception to these general observations is that the maximum cloud mixing ratio is present for the midrange value of CCN concentration of 500 cm^{-3}. This occurs because of a balance between the low and high values of CCN concentration. At low concentrations fewer and larger droplets form, which are efficiently collected by other species. At high CCN concentrations, smaller and more numerous droplets form, which are not efficiently collected but are more likely to evaporate completely. At the midrange concentration we have a balance between the number and size of droplets that form, so that some are collected and some evaporate, but neither process is as extreme as in their respective extreme simulations. As such, more cloud water remains in the simulations that tend to have a balance in these processes.

The values of cloud1 concentration in Table 3 are smaller than some observations from SPL, and the mean diameters are larger as well (Borys et al. 2000, 2003), but we note that these values are domain and time averaged over cloudy and nearly cloud-free areas; thus, they do not give information on the instantaneous cloud field. However, average droplet mean diameters are similar to those from numerous droplet distributions displayed in Pruppacher and Klett (1997). Throughout the simulations, individual clouds contained regions with domain-maximum droplet concentrations ranging from 55 cm^{-3} for low initial CCN concentrations up to 750 cm^{-3} for high initial CCN concentrations. At high CCN concentrations, instantaneous mean diameters were found around 10–15 μm [values similar to Borys et al. (2000, 2003)].

Vertical cross sections centered over SPL reveal the vertical stratification of the various hydrometeor species including the low-level cloud layer (see Fig. 6). The modeled supercooled cloud layer near SPL was shallow and extended up to about 1200 m above ground. Graupel was present in this layer also, as a result of the riming of cloud water by snow and aggregates and the development of a liquid layer on their surfaces. (The presence of a liquid layer results in the subsequent transfer to graupel.) Above the level of supercooled cloud water, ice clouds existed that contained pristine ice, snow, and aggregates. Although SPL was enshrouded by supercooled liquid cloud during the time shown in the cross section, the cloud was often glaciated and consisted primarily of ice crystals, snow, and aggregates. The presence of glaciated cloud can be attributed to a Bergeron–Findeisen process, whereby the vapor consumption by ice species occurs below water supersaturation.

5. Aerosol impact upon microphysical processes

All processes constituting source and sink terms for each hydrometeor species were examined to determine the variation in dominant processes as a result of

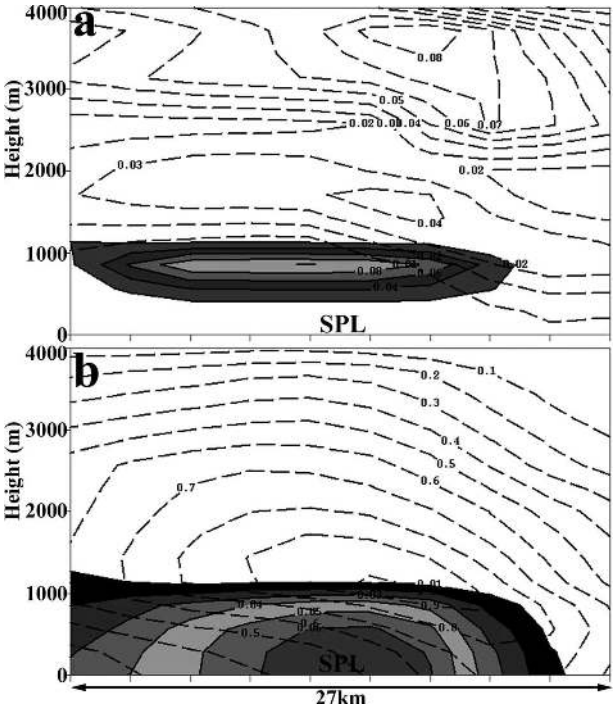

FIG. 6. Vertical west–east cross section of hydrometeor mixing ratios (g kg^{-1}) of (a) cloud1 (shaded and solid lines) and snow (dotted lines) and (b) graupel (shaded and solid lines) and aggregates (dotted lines). The cross section is taken at 1300 UTC 28 Feb, centered over SPL.

TABLE 4. Changes in sources and sinks of mixing ratio (g kg^{-1}) are given for an increase in CCN concentration (cm^{-3}) from 100 (average of expts 3, 4, and 5) to 1000 (average of expts 9, 10, and 11). All values given are domain summed and time-step averaged over the course of the 39-h simulations. For example, the cloud1 droplet category (CL1) experiences a domain-summed and time-averaged decrease in droplet-nucleated mixing ratio of 8.3×10^{-4} g kg^{-1} for the given averaged increase in CCN concentration. Only the most dominant processes are shown. The notation "xfer" signifies a hydrometeor category transfer; the other definitions are cloud2: CL2, rain: RA, pristine ice: PR, snow: SN, aggregate: AG, graupel: GR, and hail: HA.

Class	Sources	Amount	Sinks	Amount	Net
CL1	Droplet nucleation	-8.30×10^{-4}	Rimed by AG	-5.59×10^{-4}	4.40×10^{-5}
	Vapor deposition	-3.39×10^{-4}	Evaporation	-4.33×10^{-4}	
			Rimed by GR	-1.18×10^{-4}	
			Rimed by SN	-1.03×10^{-4}	
CL2	Droplet nucleation	-8.26×10^{-5}	Rimed by AG	-5.52×10^{-5}	1.33×10^{-6}
	Vapor deposition	-5.74×10^{-6}	Evaporation	-1.55×10^{-5}	
			Rimed by GR	-1.10×10^{-5}	
			Rimed by SN	-7.97×10^{-6}	
RA	GR melting, xfer GR to RA	8.76×10^{-5}	Collected by GR	2.97×10^{-5}	2.96×10^{-5}
	HA melting, xfer HA to RA	2.23×10^{-5}	AG collect RA, xfer RA to HA	1.64×10^{-5}	
	GR collect RA, xfer GR to RA	-1.14×10^{-5}	Evaporation	1.57×10^{-5}	
	AG collect RA, xfer AG to RA	5.80×10^{-6}	Collected by AG	1.29×10^{-5}	
PR and SN	Vapor deposition	-1.17×10^{-3}	Collected by AG	-7.96×10^{-4}	-6.00×10^{-6}
			Evaporation	-3.39×10^{-4}	
			Collected by GR	-1.69×10^{-5}	
			Rime CL1, xfer PR, SN to GR	-1.11×10^{-5}	
AG	Vapor deposition	-6.83×10^{-4}	Evaporation	-2.01×10^{-3}	8.97×10^{-4}
	Collect SN	-6.21×10^{-4}	Collected by GR	-4.43×10^{-4}	
	Collect PR	-1.76×10^{-4}	Melting	1.28×10^{-4}	
	Collect RA	1.29×10^{-4}	Rime CL1, xfer AG to GR	-5.63×10^{-5}	
			Collect RA, xfer AG to HA	1.69×10^{-5}	
GR	AG rime CL1, xfer CL1 to GR	-5.59×10^{-4}	Collected by HA	-3.84×10^{-4}	-6.65×10^{-4}
	Collect AG	-4.43×10^{-4}	Evaporation	-2.43×10^{-4}	
	AG melt, xfer AG to GR	1.28×10^{-4}	Melting	8.76×10^{-5}	
	Rime CL1	-1.18×10^{-4}	Collect RA, xfer GR to RA	-1.14×10^{-5}	
	SN rime CL1, xfer CL1 to GR	-1.03×10^{-4}			
	AG rime CL1, xfer AG to GR	-5.63×10^{-5}			
	AG rime CL2, xfer CL2 to GR	-5.52×10^{-5}			
	Collect RA	2.97×10^{-5}			
	Collect SN	-1.71×10^{-5}			
	SN rime CL1, xfer SN to GR	-1.11×10^{-5}			
	Rime CL2	-1.10×10^{-5}			
HA	Collect GR	-3.84×10^{-4}	Melting	2.23×10^{-5}	-3.73×10^{-4}
	AG collect RA, xfer AG to HA	1.69×10^{-5}			
	AG collect RA, xfer RA to HA	1.64×10^{-5}			

changes in aerosol concentrations. Table 4 reveals the major processes that are altered because of an increase in initial CCN concentration from 100 to 1000 cm^{-3} (averaged over GCCN concentrations). Table 5 reveals the processes that are important because of an increase in GCCN concentration from 10^{-5} to 10^{-2} cm^{-3} (averaged over CCN concentrations). Changes in these processes help to explain the reasons for variations in surface accumulated precipitation and accumulation of each hydrometeor type (see Fig. 7). Positive (negative) values in Tables 4 and 5 indicate an increase (decrease) in the mixing ratio source or sink term as a result of a given process for an increase in CCN or GCCN concentration. All given changes in hydrometeor mixing ratio (g kg^{-1}) are domain summed and time-step averaged. For example, when CCN are increased (Table 4), the droplet nucleation for cloud1 (primary source term) is reduced by 8.30×10^{-4} g kg^{-1}, and the riming by aggregates for cloud1 (primary sink term) is decreased by 5.59×10^{-4} g kg^{-1}. The total change in sources and sinks results in a total net increase in cloud1 production of 4.40×10^{-5} g kg^{-1}. Tables 4 and 5 both follow this pattern. Only those processes that exhibit relatively large changes are given; other processes not shown are

TABLE 5. Same as Table 4, but for an increase in GCCN concentration (cm^{-3}) from 10^{-5} (average of expts 5, 8, and 11) to 10^{-2} (average of expts 4, 7, and 10).

Class	Sources	Amount	Sinks	Amount	Net
CL1	Droplet nucleation	-7.44×10^{-4}	Evaporation	-2.15×10^{-4}	1.70×10^{-5}
	Vapor deposition	2.85×10^{-4}	Rimed by AG	-1.96×10^{-4}	
			Rimed by GR	-3.60×10^{-5}	
			Rimed by SN	-2.90×10^{-5}	
CL2	Droplet nucleation	8.29×10^{-5}	Rimed by AG	5.40×10^{-5}	-1.18×10^{-6}
	Vapor deposition	4.41×10^{-6}	Evaporation	1.58×10^{-5}	
			Rimed by GR	1.09×10^{-5}	
			Rimed by SN	7.79×10^{-6}	
RA	GR melting, xfer GR to RA	-1.62×10^{-4}	Collected by GR	8.14×10^{-5}	-1.56×10^{-4}
	HA melting, xfer HA to RA	7.06×10^{-5}	Collected by AG	4.32×10^{-5}	
	GR collect RA, xfer GR to RA	1.66×10^{-5}	Evaporation	-2.59×10^{-5}	
	AG collect RA, xfer AG to RA	1.91×10^{-6}	AG collect RA, xfer RA to HA	-1.51×10^{-5}	
PR and SN	Vapor deposition	-1.46×10^{-4}	Collected by AG	-7.39×10^{-5}	1.95×10^{-5}
	Collect RA	1.39×10^{-5}	Evaporation	-7.27×10^{-5}	
			Rime CL1, xfer PR, SN to GR	-3.17×10^{-6}	
			Collected by GR	-1.78×10^{-6}	
AG	Collect SN	-4.59×10^{-5}	Evaporation	-2.90×10^{-4}	3.01×10^{-4}
	Collect RA	4.32×10^{-5}	Collected by GR	9.96×10^{-5}	
	Collect PR	-2.77×10^{-5}	Melting	-7.71×10^{-5}	
	Vapor deposition	2.31×10^{-5}	Collect RA, xfer AG to HA	-2.13×10^{-5}	
			Rime CL1, xfer AG to GR	-1.96×10^{-5}	
GR	SN rime CL1, xfer CL1 to GR	-2.92×10^{-4}	Collected by HA	3.66×10^{-4}	-5.51×10^{-4}
	AG rime CL1, xfer CL1 to GR	-1.95×10^{-4}	Melting	-1.62×10^{-4}	
	Collect RA	8.14×10^{-5}	Evaporation	-6.27×10^{-5}	
	Collect AG	8.04×10^{-5}	Collect RA, xfer GR to RA	1.66×10^{-5}	
	AG melt, xfer AG to GR	-7.68×10^{-5}			
	AG rime CL2, xfer CL2 to GR	$5.40 \times 10^{-5}5$			
	Rime CL1	-3.61×10^{-5}			
	AG rime CL1, xfer AG to GR	-1.96×10^{-5}			
	Rime CL2	1.09×10^{-5}			
HA	Collect GR	3.66×10^{-4}	Melting	7.06×10^{-5}	2.56×10^{-4}
	AG collect RA, xfer AG to HA	-2.13×10^{-5}			
	AG collect RA, xfer RA to HA	-1.51×10^{-5}			
	Collect AG	-3.26×10^{-6}			

of smaller magnitude and have little impact upon the total net change. Processes related to sources and sinks often make reference to changes in hydrometeor mixing ratio, number concentration, and diagnosed mean diameter (from mass–diameter power-law relations) that have been provided in Table 6.

a. Impact of CCN increase upon hydrometeor species

The most dominant changes in sources and sinks for each hydrometeor species, resulting from increased CCN number concentration, are given as follows.

Cloud1 condensate production experiences a total net increase over the course of the simulations. During the early spinup of the microphysics, the increased CCN results in enhanced acquisition of vapor for droplet nucleation. However, competition for vapor between deposition, upon all hydrometeor types, and droplet nucleation results in reduced nucleated mass following initial cloud development. As a result, though, riming of cloud1 by all ice species decreases because of the smaller droplet sizes. This averaged decrease in droplet nucleation represents the single greatest change among sources and sinks for cloud1 droplets. The decrease in source terms is less than the decrease in sink terms, thus leaving a net increase in cloud1.

Cloud2 condensate production experiences a modest net increase. The reduction in droplet nucleation is the greatest change among sources and sinks; less excess vapor is allotted for nucleation of cloud2 because of vapor competition imposed by a greater number of

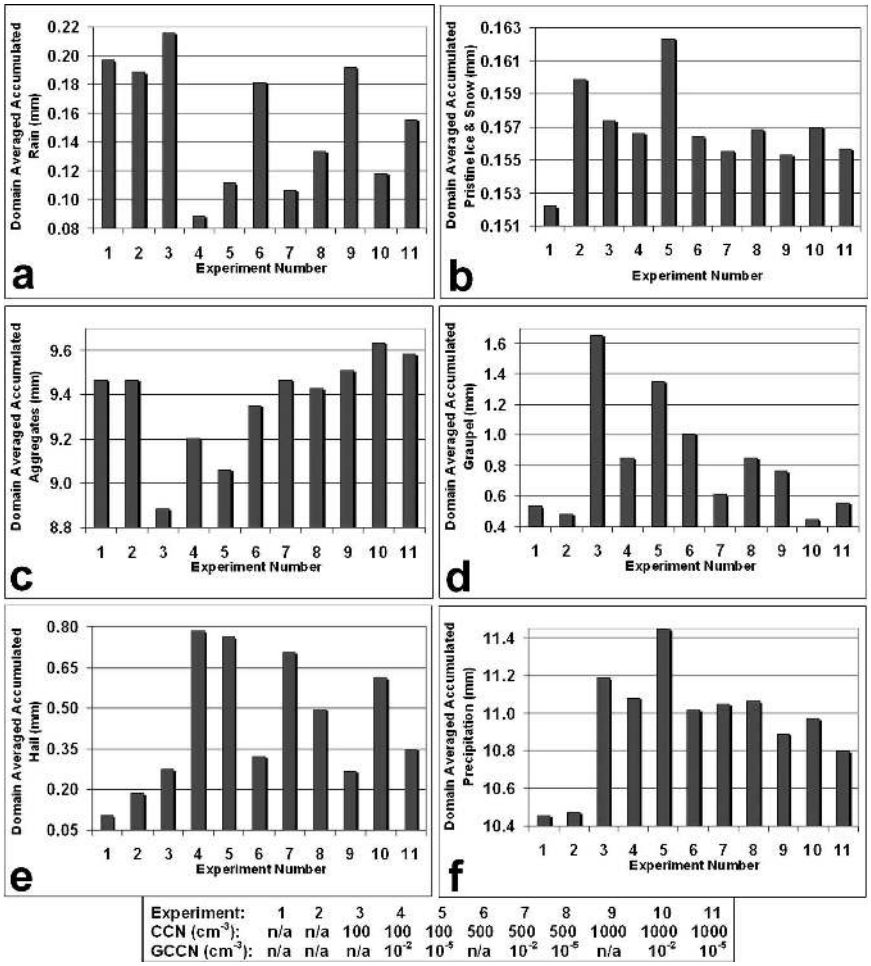

FIG. 7. Domain-averaged total liquid equivalent surface accumulation (mm) of (a) rain, (b) pristine ice and snow, (c) aggregates, (d) graupel, (e) hail, and (f) total precipitation for each of the sensitivity experiments.

CCN. However, the reduction in riming (resulting from reduced available cloud2) by the ice species offsets the reduced sources such that a small surplus persists.

Rain condensate production experiences a total net increase. The primary source term provides an increase to rain because of the melting of graupel, and the primary sink term is an increase in collection by graupel. These two processes mutually affect one another, but the increase in melted graupel is ~3 times its collection. A slightly larger graupel mean diameter increases the amount of graupel that falls below the freezing level and melts. The increased collection of rain by graupel is due to higher number concentrations of rain droplets with smaller mean diameters, as well as the increase in graupel size. The greater fall speed differential allows graupel to collect more raindrops. The net result leads to an increase in averaged rainfall at the surface for an increase in CCN. A surface analysis of graupel, hail, and rain reveal collocated regions of increased rainfall and decreased graupel and hail.

Pristine ice and snow experience a modest net decrease in condensate production. The very dominant source term is vapor deposition, which experiences a relatively large decrease because of vapor competition introduced by the increase in CCN. However, a reduction in sink terms (primarily reduced collection by aggregates) tends to offset the reduced growth such that only a small deficit results. Reduced collection by aggregates results from the presence of fewer and smaller ice and snow crystals. The net result translates to a decrease in surface accumulation of ice and snow.

Aggregates experience the greatest net change of all species with an overall increase in condensate production. Of the source terms, there is a decrease in vapor deposition growth and a decrease in collection of pristine ice and snow (because of their smaller size and

TABLE 6. Percentage change in hydrometeor characteristics resulting from the increase in CCN and GCCN concentration (cm^{-3}) from 100 (average of expts 3, 4, and 5) to 1000 (average of expts 9, 10, and 11) and from 10^{-5} (average of expts 5, 8, and 11) to 10^{-2} (average of expts 4, 7, and 10), respectively. Hydrometeor properties are time averaged and domain averaged over grid cells with hydrometeor mixing ratio greater than 10^{-6} g kg^{-1}.

Hydrometeor property	Percent change with increased CCN	Percent change with increased GCCN
Rain mixing ratio	44.44%	−48.84%
Rain concentration	37.09%	−56.15%
Rain mean diameter	−31.58%	−52.19%
Pristine ice mixing ratio	−4.72%	−0.21%
Pristine ice concentration	−4.38%	−0.43%
Pristine ice mean diameter	−0.21%	−0.17%
Snow mixing ratio	−5.44%	−0.45%
Snow concentration	−5.23%	−0.57%
Snow mean diameter	−0.24%	−0.21%
Aggregate mixing ratio	−0.33%	−0.06%
Aggregate concentration	−3.65%	−1.03%
Aggregates mean diameter	−0.02%	−0.14%
Graupel mixing ratio	−38.40%	−21.86%
Graupel concentration	−27.54%	−14.26%
Graupel mean diameter	3.41%	−1.18%
Hail mixing ratio	15.87%	9.67%
Hail concentration	38.72%	−41.06%
Hail mean diameter	−13.52%	−21.92%

concentration). However, a greater magnitude decrease in sink terms results in the net increase in available condensate. Of the sink terms, the relatively large decrease in evaporation of aggregates offsets the reduced aggregate growth. Reduced vapor deposition and evaporation can be partly attributed to a reduction in number concentration. Aggregates inherently exhibit a large surface area–to-volume ratio, which imposes a relatively large impact, relative to other hydrometeor types, upon vapor diffusional growth because of changes in number and size. Furthermore, in the case of increased CCN, it was found that the production of total hydrometeor condensate was reduced because of the initial competition for vapor and subsequent reduced riming growth of droplets; as such, the ambient vapor mixing ratio (and relative humidity) tended to be higher. This more-saturated environment contributes to the reduction in evaporation. The total net increase translates into an increase in aggregate accumulation in the higher terrain of Colorado above the freezing level.

Graupel experiences the greatest net decrease in production among hydrometeor types. There are many sources that contribute to the graupel category, with no single change determining the overall net difference. However, the sum of all riming processes largely controls the outcome. The single greatest graupel source term change is the reduction in the transfer to graupel of mixed-phased hydrometeors. The reduction in mixed-phased hydrometeors results from the reduced riming of cloud1 by aggregates (because of smaller cloud1 sizes). If aggregates rime enough cloud water, the water-to-ice ratio is enough that the mixed-phase mass should be treated as graupel rather than aggregates (which are considered to be completely frozen). This mixed-phase mass (part cloud1, part aggregate) is transferred to the graupel category. Of the sink terms, the reduction in the amount of graupel collected by hail is the primary process. This collection is decreased because of the reduced number concentration of graupel and a reduced fall speed differential between graupel and hail resulting from the convergence of their relative mean diameters. The total net decrease ultimately results in less graupel accumulation at the surface.

Hail also experiences a net decrease in condensate production. The reduced collection of graupel (discussed above) determines the net result by an order of magnitude. An increase in melting is the sole influential sink term for hail. Greater melting is attributed to greater hail number concentration as well as a smaller hail mean diameter, resulting in longer residence times below the freezing level. A net decrease results in a reduction in surface accumulation of hail.

b. Impact of GCCN increase upon hydrometeor species

The most dominant changes in sources and sinks for each hydrometeor species, resulting from the increased GCCN number concentration, are given as follows.

Cloud1 condensate production experiences a total net increase over the course of the simulations, but to a lesser degree than for increased CCN concentrations. The addition of GCCN creates a competition for vapor available for nucleation, such that less is allotted to the cloud1 category. As such, the reduction of cloud1 nucleation is the single most influential process among changes in sources and sinks. However, reduced nucleation results in smaller cloud1 droplets, which imposes a reduction in riming of cloud1 by the ice species. The reduction in sinks for cloud1 is greater than the reduction in sources, thus, leaving a net surplus.

Cloud2 undergoes a net reduction in the average production of condensate. The addition of GCCN results in a relatively large increase in cloud2 nucleation whose magnitude is greater than all other processes that influence cloud2. However, this increase in available cloud2 results in its increased evaporation and collection by the ice species. Larger and more numerous cloud2 droplets have higher collection efficiencies and are readily scavenged by aggregates and graupel. The sinks

of cloud2 outweigh the sources, thus leading to a small net decrease.

Rain responds in an opposite manner to increased CCN, such that increased GCCN results in a net decrease in rain condensate production. In this case, less graupel mass is melting to rain while more rain is being collected by graupel. The reduction in melted graupel is primarily a function of less graupel condensate being available for melting because of its increased collection by hail. The increased collection of rain by graupel is due to smaller rain mean diameters; a greater fall speed differential between rain and graupel increases the rain volume swept out by graupel and increases the collection rate. The net decrease in rain sources and increase in sinks produces a net decrease in rain production and reduced rainfall at the surface. In this case of increased GCCN concentration, the surface accumulation of hail is increased at the expense of both rain and graupel.

Pristine ice and snow also respond in an opposite manner to increased CCN, with a relatively moderate net increase in condensate production resulting from changes in sources and sinks. As before, for these species, the dominant reduction in vapor depositional growth is due to increased competition for available vapor beyond saturation because of the introduction of more GCCN. The sink terms, primarily collection by aggregates and evaporation, are reduced to a greater degree than are the source terms. For both pristine ice and snow, the number concentrations and mean diameters are reduced, thus resulting in their decreased collection by the other ice species. This condition poses an interesting response because the surface accumulation of pristine ice and snow is slightly reduced despite a small increase in net condensate production. This is not difficult to imagine, however, because pristine ice and snow inherently have very slow fall speeds; though an increase in condensate exists, the mean diameters are slightly smaller. Smaller sizes and slower fall speeds would explain the reduction in surface accumulation.

Aggregates experience a net increase in condensate production, but it is 1/3 of the size of the increase seen for an increase in CCN concentration. Although the hydrometeor collection and vapor deposition source terms nearly offset one another, the substantial decrease in evaporation of aggregates is the dominant factor in providing and retaining more mass in this ice category. Decreased evaporation results primarily from the combined influence of the large surface area–to-volume ratio of aggregates and the more saturated ambient environment characterized by higher vapor mixing ratios. The small reduction in aggregate number concentration would further contribute to the evaporation reduction. The total net increase in aggregate production translates into a net increase in their surface accumulation.

Graupel condensate production undergoes the greatest change of all species because of the increase in GCCN, with a net decrease of similar magnitude to the case of increased CCN. Similar to before, the primary changes in source terms constitute a reduction resulting from reduced riming of cloud1 droplets by snow and aggregates and their subsequent transition to graupel because of the liquid contribution. This process relates back to reduced cloud1 nucleation and smaller cloud1 droplets characterized by smaller collection efficiencies. The sink terms are dominated by an increase in the collection of graupel by hail because of greater available hail mixing ratio. The resulting net decrease from reduced sources and enhanced sinks translates into a decrease in graupel accumulation at the surface.

Hail condensate production experiences a net increase when GCCN concentration is increased; this behavior is opposite to the case of increased CCN. Of the source terms, the increased collection of graupel by hail has the greatest impact by an order of magnitude. The only major sink term for hail is melting. Although melting is slightly increased, because of increased available hail mass and smaller hail diameters, the magnitude is small relative to collection growth. Increased collection of graupel can be attributed to an increase in total hail mass. The transfer of graupel to hail produces an increase in hail condensate and increased accumulation at the surface.

c. Impacts of ice nuclei variability

All of the above experiments were performed using the Meyers et al. (1992) formulation for estimating activation of IN. However, IN variability, while not the focus of this paper, is another source of variability in the mixed-phase precipitation process. During recent winters, including 2004, Demott et al. (2003; P. J. Demott 2005, personal communication) obtained measurements of IN concentrations at SPL. Those measurements suggest that the Meyers formulation may be overactivating the number of IN that result in ice crystal formation. The Meyers formula activates IN with concentrations from 0.008 to 1.0 cm^{-3} at 20%–60% ice supersaturation. The measurements of Demott et al. (2003) suggest concentrations from 0.002 to 0.008 cm^{-3} at 20%–60% ice supersaturation. We performed one simulation that is identical to experiment 8 (CCN concentration = 500 cm^{-3} and GCCN concentration = 10^{-2} cm^{-3}) but with the reduced IN activation rate, so as to examine the influence of IN variability on orographic precipitation over Colorado. It was suspected that the reduction in IN activation might result in in-

creased cloud mixing ratio, but this was not the case; such changes were minor. There was, however, a reduction in domain-averaged precipitation by 0.25 mm and domain-summed precipitated water equivalent by 21×10^6 m^3. Reduced IN activation results in reduced ice water content and reduced precipitating ice hydrometeors. Although the new IN data suggest the need for a refined IN activation formula, Demott et al. (2003) note that further data are needed before recommending updated parameterizations of IN within microphysical models.

6. Summary and conclusions

The mesoscale RAMS was used to perform a series of 11 simulations whose purpose was to assess the model performance and to examine model sensitivity and variability in a wintertime snow event that occurred during 28–29 February over the mountains of Colorado. The real-time version 4.3 of RAMS runs daily in a forecast mode with its nested domain of 3-km grid spacing focused over the mountains and western plains of Colorado. The real-time version of RAMS has changed little since version 4.3 was released in 2000, whereas a new parameterization for cloud-droplet nucleation from an initialized field of CCN and GCCN has been implemented in the research version of RAMS (Part I). It has been suspected that the default representation of cloud-droplet formation in the model is too simplistic and inflexible with respect to modeling different air masses. The new cloud-droplet parameterization allows for flexibility in droplet formation by allowing the user to specify aerosol concentration and size (Part I). The fraction of aerosols that activate and result in cloud-droplet formation is a function of aerosol concentration and size, ambient temperature, and vertical velocity.

In this study we examined the range of model realizations that resulted from initializing the model with relative extremes in the CCN and GCCN concentration, as well as with the default droplet formation scheme that the real-time model currently uses. Comparisons between the results of the sensitivity tests and observations from SPL and several SNOTEL stations also provided insight into the potential for forecast improvement with use of the newer aerosol/cloud-droplet parameterization. The following is a summary of key findings and relationships determined from model analyses:

1) The ensemble of simulations utilizing the new aerosol/cloud-droplet parameterization generally produced the best forecasts of atmospheric conditions recorded at SPL and precipitation at surrounding SNOTEL sites. Among the sensitivity experiments, the total domain-averaged accumulated precipitation varied by a maximum range of ~1.0 mm (~10% variability). At the Storm Peak Laboratory location, the total precipitation variability reached 5 mm (~20%) among simulations. The range of modeled precipitation extremes over the SNOTEL sites in northern Colorado revealed a variation up to ~30% depending upon the initial aerosol concentration. The total accumulated precipitation was reduced as the aerosol concentration was increased.
2) Increasing the CCN concentration resulted in formation of a greater number of small cloud1 and cloud2 droplets, which reduced the relative importance of vapor depositional growth of droplets, pristine ice, snow, and aggregates because of enhanced competition for vapor among cloud droplets. This effect also decreased the riming of cloud1and cloud2 by the ice species as a result of smaller riming efficiencies, and it increased rainfall at lower elevations at the expense of increased melting of hail and graupel. Aggregate accumulation also increased despite reduced collection growth; this is a result of reduced evaporation that was limited by higher ambient vapor mixing ratio and relative humidity. Aggregates are most strongly affected by such changes because of their relatively large surface area–to-volume ratio. These results, indicating formation of smaller, numerous droplets and reduced riming, are consistent with the observations of Borys et al. (2000, 2003) and Hindman et al. (1994).
3) Increasing the number of GCCN resulted in formation of a greater number of cloud2 droplets as well as fewer and smaller cloud1 droplets; this is due to competition for vapor growth. This resulted in decreased (increased) collisional growth of other species by cloud1 (cloud2) because of changes in collection efficiency. Because collisional growth through cloud1 droplets is reduced and cloud1 mixing ratio is typically much greater than that in cloud2, the growth and surface accumulation of rain, pristine ice and snow, and graupel is reduced. In contrast, aggregate accumulation increases because of reduced evaporation within a more saturated environment. Hail accumulation also increased as a result of greater collection of graupel.
4) Total precipitation accumulation was reduced as CCN concentration was increased because of greater competition for vapor growth and reduced collection of smaller cloud droplets. An increase in GCCN produces opposite effects depending upon the CCN concentration. At high CCN concentrations, the addition of GCCN helps to speed hydrometeor growth

through enhanced collision/coalescence, thus resulting in enhanced surface precipitation [similar to results from Johnson (1982), Mather (1991), and Feingold et al. (1999)]. At low CCN concentrations, additional GCCN cause an increase in vapor competition for nucleation and deposition, thus limiting droplet sizes and collection growth. This tends to reduce the total surface precipitation.

We emphasize the range of model accumulated precipitation that results, depending upon how the formation of cloud droplets is treated in the model microphysics and what initial aerosol concentrations are specified. Furthermore, the treatment of droplet formation and variations in aerosol concentrations produce differing degrees of model response to liquid-phase and ice-phase processes, which produce relative variations in accumulation of the different hydrometeor species. Comparisons made with the surface precipitation accumulation suggest that the default cloud-droplet nucleation scheme used in the current real-time RAMS tends to represent an extreme in droplet formation. The results presented here favor improved model forecasting by representing more realistic droplet formation. Ongoing research in our group, used to refine our treatment of modeled aerosols, includes developing a regional to global cloud-nucleating aerosol source, sink, and transport model and development of satellite retrieval of these aerosols.

Acknowledgments. We thank Dr. Randy Borys for providing us with the real-time data from SPL and for his insight and suggestions regarding this manuscript. This research was supported by the National Science Foundation under Grant ATM-0215367.

REFERENCES

Borys, R. D., D. H. Lowenthal, and D. L. Mitchell, 2000: The relationships among cloud microphysics, chemistry, and precipitation rate in cold mountain clouds. *Atmos. Environ.,* **34,** 2593–2602.

——, ——, S. A. Cohn, and W. O. J. Brown, 2003: Mountaintop and radar measurements of anthropogenic aerosol effects on snow growth and snowfall rate. *Geophys. Res. Lett.,* **30,** 1538, doi:10.1029/2002GL016855.

Clark, T. L., and W. D. Hall, 1983: A cloud physical parameterization method using movable basis functions: Stochastic coalescence parcel calculations. *J. Atmos. Sci.,* **40,** 1709–1728.

Cotton, W. R., and Coauthors, 2003: RAMS 2001: Current status and future directions. *Meteor. Atmos. Phys.,* **82,** 5–29.

Demott, P. J., D. J. Cziczo, A. J. Prenni, D. M. Murphy, S. M. Kreidenweis, D. S. Thomson, R. Borys, and D. C. Rogers, 2003: Measurements of the concentration and composition of nuclei for cirrus formation. *Proc. Natl. Acad. Sci. USA,* **100,** 14 655–14 660.

Dudhia, J., 1989: Numerical study of convection observed during the winter monsoon experiment using a mesoscale two-dimensional model. *J. Atmos. Sci.,* **46,** 3077–3107.

Feingold, G., S. Tzivion, and Z. Levin, 1988: Evolution of raindrop spectra. Part I: Solution to the stochastic collection/breakup equation using the method of moments. *J. Atmos. Sci.,* **45,** 3387–3399.

——, W. R. Cotton, S. Kreidenweis, and J. Davis, 1999: The impact of giant cloud condensation nuclei on drizzle formation in stratocumulus: Implications for cloud radiative properties. *J. Atmos. Sci.,* **56,** 4100–4117.

Ferrier, B. S., W. K. Tao, and J. Simpson, 1995: A double-moment multiple-phase four-class bulk ice scheme. Part II: Simulations of convective storms in different large-scale environments and comparisons with other bulk parameterizations. *J. Atmos. Sci.,* **52,** 1001–1033.

Fitzgerald, J. W., and P. A. Spyers-Duran, 1973: Changes in cloud nucleus concentration and cloud droplet size distribution associated with pollution from St. Louis. *J. Appl. Meteor.,* **12,** 511–516.

Heymsfield, A. J., and R. M. Sabin, 1989: Cirrus crystal nucleation by homogeneous freezing of solution droplets. *J. Atmos. Sci.,* **46,** 2252–2264.

Hindman, E. E., M. A. Campbell, and R. D. Borys, 1994: A ten-winter record of cloud-droplet physical and chemical properties at a mountaintop site in Colorado. *J. Appl. Meteor.,* **33,** 797–807.

Hobbs, P. V., M. K. Politovich, and L. F. Radke, 1980: The structures of summer convective clouds in eastern Montana. I: Natural clouds. *J. Appl. Meteor.,* **19,** 645–663.

Hong, S. Y., H. M. H. Juang, and Q. Zhao, 1998: Implementation of prognostic cloud scheme for a regional spectral model. *Mon. Wea. Rev.,* **126,** 2621–2639.

Hsie, E. Y., and R. A. Anthes, 1984: Simulations of frontogenesis in a moist atmosphere using alternative parameterizations of condensation and precipitation. *J. Atmos. Sci.,* **41,** 2701–2716.

Johnson, D. B., 1982: The role of giant and ultragiant aerosol particles in warm rain initiation. *J. Atmos. Sci.,* **39,** 448–460.

Kain, J. S., and J. M. Fritsch, 1990: A one-dimensional entraining/detraining plume model and its application in convective parameterization. *J. Atmos. Sci.,* **47,** 2784–2802.

——, and ——, 1992: The role of the convective "triggering function" in numerical forecasts of mesoscale convective systems. *Meteor. Atmos. Phys.,* **49,** 93–106.

——, and ——, 1993: Convective parameterization for mesoscale models: The Kain-Fritsch scheme. *The Representation of Cumulus Convection in Numerical Models, Meteor. Monogr.*, No. 46, Amer. Meteor. Soc., 165–170.

Kessler, E., 1969: *On the Distribution and Continuity of Water Substance in Atmospheric Circulations*. *Meteor. Monogr.*, No. 32, Amer. Meteor. Soc., 84 pp.

Marshall, J. S., and W. Palmer, 1948: The distribution of raindrops with size. *J. Meteor.,* **5,** 165–166.

Mather, G. K., 1991: Coalescence enhancement in large multicell storms caused by the emissions from a Kraft paper mill. *J. Appl. Meteor.,* **30,** 1134–1146.

Mellor, G. L., and T. Yamada, 1974: A hierarchy of turbulence closure models for planetary boundary layers. *J. Atmos. Sci.,* **31,** 1791–1806.

Meyers, M. P., P. J. DeMott, and W. R. Cotton, 1992: New primary ice-nucleation parameterizations in an explicit cloud model. *J. Appl. Meteor.,* **31,** 708–721.

——, R. L. Walko, J. Y. Harrington, and W. R. Cotton, 1997: New

RAMS cloud microphysics parameterization. Part II. The two-moment scheme. *Atmos. Res.,* **45,** 3–39.

Peilke, R. A., Sr., and Coauthors, 1992: A comprehensive meteorological modeling system—RAMS. *Meteor. Atmos. Phys.,* **49,** 69–91.

Pruppacher, H., and J. Klett, 1997: *Microphysics of Clouds and Precipitation*. 2d ed. Kluwer Academic, 954 pp.

Reisner, J., R. M. Rasmussen, and R. T. Bruintjes, 1998: Explicit forecasting of supercooled liquid water in winter storms using the MM5 mesoscale model. *Quart. J. Roy. Meteor. Soc.,* **124,** 1071–1107.

Saleeby, S. M., and W. R. Cotton, 2004: A large droplet mode and prognostic number concentration of cloud droplets in the Colorado State University Regional Atmospheric Modeling System (RAMS). Part I: Module descriptions and supercell test simulations. *J. Appl. Meteor.,* **43,** 182–195.

Smagorinsky, J., 1963: General circulation experiments with the primitive equations. *Mon. Wea. Rev.,* **91,** 99–164.

Souto, M. J., C. F. Balseiro, V. Pérez-Muñuzuri, M. Xue, and K. Brewster, 2003: Impact of cloud analysis on numerical weather prediction in the Galician region of Spain. *J. Appl. Meteor.,* **42,** 129–140.

Tao, W. K., J. Simpson, and M. McCumber, 1989: An ice-water saturation adjustment. *Mon. Wea. Rev.,* **117,** 231–235.

Tzivion, S., G. Feingold, and Z. Levin, 1987: An efficient numerical solution to the stochastic collection equation. *J. Atmos. Sci.,* **44,** 3139–3149.

Verlinde, J., P. J. Flatau, and W. R. Cotton, 1990: Analytical solutions to the collection growth equation: Comparison with approximate methods and application to cloud microphysics parameterization schemes. *J. Atmos. Sci.,* **47,** 2871–2880.

Walko, R. L., W. R. Cotton, M. P. Meyers, and J. Y. Harrington, 1995: New RAMS cloud microphysics parameterization: Part I. The single-moment scheme. *Atmos. Res.,* **38,** 29–62.

——, ——, ——, and ——, 2000: Efficient computation of vapor and heat diffusion between hydrometeors in a numerical model. *Atmos. Res.,* **53,** 171–183.

Warner, J., 1969: The microstructure of cumulus cloud. Part I. General features of the droplet spectrum. *J. Atmos. Sci.,* **26,** 1049–1059.

——, and S. Twomey, 1967: The production of cloud nuclei by cane fires and the effect on cloud droplet concentration. *J. Atmos. Sci.,* **24,** 704–706.

Ziegler, C. L., 1985: Retrieval of thermal and microphysical variables in observed convective storms. Part 1: Model development and preliminary testing. *J. Atmos. Sci.,* **42,** 1487–1509.